


Article

Alleviation of Ultrafiltration Membrane Fouling by ClO₂ Pre-Oxidation: Fouling Mechanism and Interface Characteristics

Bin Liu ¹, Meng Wang ¹, Kaihan Yang ^{2,*}, Guangchao Li ^{1,*} and Zhou Shi ¹

¹ Key Laboratory of Building Safety and Energy Efficiency, Ministry of Education, Department of Water Engineering and Science, College of Civil Engineering, Hunan University, Changsha 410082, China; ahxclb@163.com (B.L.); wmnzzd@163.com (M.W.); zhous@hnu.edu.cn (Z.S.)

² People's Government Office, Bijiang District, Tongren 554300, China

* Correspondence: ykheart@live.com (K.Y.); liguangchao@hnu.edu.cn (G.L.)

Abstract: In order to alleviate membrane fouling and improve removal efficiency, a series of pre-treatment technologies were applied to the ultrafiltration process. In this study, ClO₂ was used as a pre-oxidation strategy for the ultrafiltration (UF) process. Humic acid (HA), sodium alginate (SA), and bovine serum albumin (BSA) were used as three typical organic model foulants, and the mixture of the three substances was used as a representation of simulated natural water. The dosages of ClO₂ were 0.5, 1, 2, 4, and 8 mg/L, with 90 min pre-oxidation. The results showed that ClO₂ pre-oxidation at low doses (1–2 mg/L) could alleviate the membrane flux decline caused by humus, polysaccharides, and simulated natural water, but had a limited alleviating effect on the irreversible resistance of the membrane. The interfacial free energy analysis showed that the interaction force between the membrane and the simulated natural water was also repulsive after the pre-oxidation, indicating that ClO₂ pre-oxidation was an effective way to alleviate cake layer fouling by reducing the interaction between the foulant and the membrane. In addition, ClO₂ oxidation activated the hidden functional groups in the raw water, resulting in an increase in the fluorescence value of humic analogs, but had a good removal effect on the fluorescence intensity of BSA. Furthermore, the membrane fouling fitting model showed that ClO₂, at a low dose (1 mg/L), could change the mechanism of membrane fouling induced by simulated natural water from standard blocking and cake layer blocking to critical blocking. Overall, ClO₂ pre-oxidation was an efficient pretreatment strategy for UF membrane fouling alleviation, especially for the fouling control of HA and SA at low dosages.

Keywords: ultrafiltration; ClO₂ pre-oxidation; natural organic matter; separation performance; interfacial free energy; membrane fouling model



Citation: Liu, B.; Wang, M.; Yang, K.; Li, G.; Shi, Z. Alleviation of Ultrafiltration Membrane Fouling by ClO₂ Pre-Oxidation: Fouling Mechanism and Interface Characteristics. *Membranes* **2022**, *12*, 78. <https://doi.org/10.3390/membranes12010078>

Academic Editor: Alejandro Ruiz García

Received: 9 December 2021

Accepted: 5 January 2022

Published: 10 January 2022

Publisher's Note: MDPI stays neutral with regard to jurisdictional claims in published maps and institutional affiliations.



Copyright: © 2022 by the authors. Licensee MDPI, Basel, Switzerland. This article is an open access article distributed under the terms and conditions of the Creative Commons Attribution (CC BY) license (<https://creativecommons.org/licenses/by/4.0/>).

1. Introduction

Formed as a result of the interaction between the hydrological cycle, the biosphere, and the lithosphere, natural organic matter (NOM) is commonly found in surface water and groundwater, with diverse distribution patterns [1]. Recently, scholars have observed that the content of NOM in water bodies is increasing, accompanied by severe seasonal changes, and can absorb ultraviolet rays to protect harmful substances, such as pathogens, and reduce the self-purification capacity of surface water [2,3]. In addition, Bond [4] et al. reported that NOM is the precursor of disinfection byproducts such as trihalomethanes (THMs) and haloacetic acids (HAAs). Therefore, NOM can inevitably pose a threat to the operation of water plants. Some components of NOM are collectively referred to as humus, because they have no separate chemical formulae [5]. Lipczynska-Kochany et al. [2] found that humus could be divided into humin, humic acid (HA), and fulvic acid (FA) according to molecular weight, among which HA is considered to be the dominant component of humus. Nevertheless, HA is prone to forming stronger toxic complexes with heavy metals

in water [6,7]. Moreover, other types of organics—such as polysaccharides and proteins—also present thorny problems for water treatment. Therefore, it is urgent and necessary to study the removal of NOM in water treatment.

At present, the methods for removing NOM include coagulation [8,9], adsorption [10], advanced oxidation [11], and membrane separation technology [12,13]. However, these methods each have their own shortcomings or application limitations. For example, the use of inorganic coagulants such as aluminum salts or iron salts can only remove part of the NOM. Furthermore, although common adsorbents such as activated carbon can effectively remove NOM, it is difficult to regenerate and recover the adsorption capacity, and the risk of secondary pollution of the water body is also a tricky issue.

Unlike the previous methods, ultrafiltration (UF) can effectively remove low-molecular-weight NOM, and is a small-footprint treatment process, representing an efficient and stable separation technology through size exclusion [14,15]. At present, in order to realize the sustainable development of membranes and improve their anti-pollution properties and durability, many novel materials have been applied, such as sustainable polymer [16], mor-denite zeolite [17], poly(vinyl alcohol) [18], etc. However, due to the complex structure, high molecular weight, and strong adsorption of the membrane, the organic molecules cause membrane fouling in the membrane surface and pores more easily. Therefore, during the UF process application, membrane fouling caused by organics should be highlighted [19,20].

To alleviate fouling of ultrafiltration membranes caused by NOM, a variety of pre-treatment technologies have been probed in the past several years [21–24]. Advanced pre-oxidation is considered to be an attractive method among the various pretreatment strategies. For example, the redox point of ozone is $E_0 = 2.076$ V, which can effectively change the nature of foulants and degrade membrane foulants. However, due to problems such as strong oxidation and poor selectivity, this pretreatment method may have the potential to deteriorate the quality of ultrafiltered water. The permanganate pre-oxidation method is prone to producing byproducts such as MnO_2 in the pre-oxidation process, which might reduce the lifespan of the ultrafiltration membrane. As an oxidant with moderate oxidation potential, ClO_2 can better control its degree of oxidation, and has a better ability to control the generation of disinfection byproducts [25,26].

Zhong [27] et al. reported that the presence of ClO_2 reduced THMs the most, but not HAAs or HALs, in low- NH_3-N wastewater. Shao [28] et al. studied the effects of ClO_2 pre-oxidation on the formation of dichloroacetonitrile and dichloroacetamide during subsequent chloramination. It was found that ClO_2 oxidation had inverse effects on DCAN/cAm yields for hydroxybenzamides and tetracyclines. In addition, Gan et al. reported that ClO_2 selectively reacted with compounds with electron-rich moieties, such as phenols, anilines, and thiols in the case of organic compounds [29]. Therefore, the discussion of the potential of ClO_2 as UF pretreatment for NOM in water has practical and scientific significance. This paper investigated the possibility of applying ClO_2 for pre-oxidation of the UF process.

In this study, the use of ClO_2 as a pre-oxidation method was employed to explore the mitigation effect and mechanism of membrane fouling, as well as the water purification efficiency. Three typical organic compounds—humic acid, sodium alginate, and bovine serum protein—were used as model foulants to simulate various components in surface water. Initially, membrane fouling and rejection of organic compounds were investigated. In addition, the interface characteristics of the fouled membranes—including particle size distribution, zeta potential, interfacial free energy, and morphology—were comprehensively investigated.

2. Materials and Methods

2.1. Preparation of Experimental Sewage

Humic acid (HA), sodium alginate (SA; representative of polysaccharides), and bovine serum protein (BSA; representative of proteins), which obtained from alading company (Shanghai, China), were selected for use in the raw sewage for the membrane filtration

experiments. In order to obtain 1 g/L of humic acid stock solution, 1 g of solid humic acid powder was accurately weighed on a high-precision electronic balance and then dissolved in a 1000 mL beaker together with 800 mL of sodium hydroxide solution with a concentration of 0.01 mM/L. After that, the pH was adjusted to 7.0, and the whole process was carried out again on a magnetic stirrer. In order to obtain 1 g/L of sodium alginate and bovine serum protein, 1 g of sodium alginate and bovine serum protein solid powder were each weighed in a beaker, and then placed in a magnetic stirrer with heating and stirring for 24 h; lastly, the volume was adjusted to 1000 mL. The above model foulant stock solution was stored in a refrigerator at 4 °C. For the oxidation and filtration tests, the HA, SA, and BSA were all diluted to 5 mg/L, and the concentration of the three organic compounds in the mixed solution was also 5 mg/L.

2.2. Experimental Setup

The dosages of AR-grade ClO₂ were 0.5, 1, 2, 4, and 8 mg/L. The experimental sewages were pre-oxidized for 90 min. Then, 60 mL of solution was taken out for filtration experiments. Flat ultrafiltration membranes of polyethersulfone (PES, 100 kDa) were used in the filtration experiments, which were obtained from the MICRODYN-NADIR company (Wiesbaden, Germany). The ultrafiltration device maintained a constant pressure (100 kPa) with a dead-end ultrafiltration system, without stirring of the feed solution. The device consists of an ultrafilter cup, an electronic balance (NV2201ZH, Auhaus, Shanghai, China), a nitrogen cylinder, a pressure gauge, a control valve, and a computer terminal. The cleaned ultrafiltration membrane was placed at the bottom of the ultrafiltration cup, and the pressure in the ultrafiltration cup was kept low enough that the ultrafiltration cup did not leak air or water. Under this pressure, the liquid in the ultrafilter cup flowed through the silicone tube into the beaker placed on the electronic balance. The balance was set to record the weight data at intervals of 3 s. The weight data recorded by the electronic balance were then transmitted to the computer terminal through the data line in order to obtain the ultrafiltration weight data.

2.3. Membrane Fouling Assessment and Mechanism Analysis

The resistance of the ultrafiltration membrane is composed of inherent resistance, reversible resistance, and irreversible resistance [30]. It is generally believed that the reversible resistance is caused by the cake layer on the membrane surface. The reversible resistance can be greatly reduced by gently wiping the cake layer on the membrane surface with wet sponge. Irreversible resistance is usually caused by membrane pore narrowing. The specific calculation can be deduced by the Darcy formula [31,32], as shown in Equation (1):

$$J = \frac{\Delta P}{\mu(R_i + R_b + R_c)} = \frac{\Delta P}{\mu R_{tot}} \quad (1)$$

where J represents the filtration flux (L/m²·h), μ represents the dynamic viscosity (Pa·s), ΔP represents the operating pressure (Pa), R_{tot} represents the total membrane resistance (m⁻¹), R_i represents the membrane's inherent resistance (m⁻¹), R_b represents irreversible resistance (m⁻¹), and R_c represents the reversible resistance (m⁻¹). Ultrapure water filtration was used before each filtration until the flux was stable, and the steady membrane flux was denoted as J_0 . All filtration tests were performed at least 3 times. The R_i can be calculated according to Equation (2):

$$R_i = \frac{\Delta P}{\mu J_0} \quad (2)$$

At the end of filtration, the average flux of the last 3 mL was denoted as J_1 to calculate the total membrane resistance, as shown in Equation (3):

$$R_{tot} = \frac{\Delta P}{\mu J_1} \quad (3)$$

In order to calculate the irreversible resistance of the membrane, after each filtration cycle, the ultrafiltration membrane was reset in the ultrafiltration device after gently wiping the cake layer on the membrane surface with a wet sponge under water flushing, and pure water was filtered again, i.e., the stable membrane flux after cleaning was obtained, denoted as J_2 . Therefore, the irreversible resistance R_b can be calculated according to Equation (4). The reversible resistance can be calculated by subtracting the inherent resistance and irreversible resistance from the total membrane resistance.

$$R_b = \frac{\Delta P}{\mu J_2} - \frac{\Delta P}{\mu J_0} \quad (4)$$

In order to further investigate the membrane fouling mechanism during ultrafiltration, four classical fouling models were introduced, including a complete blocking model, critical blocking model, standard blocking model, and cake layer filtration model. The complete blocking model assumes that the pores of the ultrafiltration membrane are completely blocked, so that the transmembrane resistance increases. The standard blocking model assumes that the small-particle-size foulants adhere to the inner sides of the membrane pores, narrowing them and reducing the flow capacity. The critical blocking model is between the complete blocking model and the standard blocking model. The cake layer filtration model refers to the formation of a cake layer by foulants deposited on the membrane surface. Ho and Zydney [33]'s differential form model was introduced in this study to analyze and fit the flux data. The advantage of this method is that it can more intuitively analyze the fouling mechanism under different filtration times or volumes. MATLAB was used to conduct mathematical modeling for the imported data, and cubic polynomial fitting was performed for the flux data. The formulae were as follows:

$$\frac{d^2t}{dV^2} = k \left(\frac{dt}{dV} \right)^n = - \frac{1}{J^3 A^2} \frac{dJ}{dt} \quad (5)$$

$$\frac{dt}{dV} = \frac{1}{JA} \quad (6)$$

$$n = \frac{d \left[\log \left(\frac{d^2t}{dV^2} \right) \right]}{d \left[\log \left(\frac{dt}{dV} \right) \right]} \quad (7)$$

where t represents the filtration time (s), J represents the filtration flux, and V represents the total filtration volume (mL). After finding the turning point by fitting the curve, the data before and after the change point were fitted respectively to determine the leading mechanism in different groups of fouling, according to the obtained N value: when $n = 2$, it is mainly a complete blocking model; when $n = 1.5$, standard blocking plays the dominant role; when $n = 1$, it is critical blocking; when $n = 0$, it is cake layer filtration [34].

2.4. Analytical Methods

The ultraviolet absorbance (UV_{254}) was determined using an ultraviolet spectrophotometer (T6, PUXI, Beijing, China), and dissolved organic carbon (DOC) was determined using a total organic carbon analyzer (TOC-VCSH, Shimadzu, Kyoto, Japan). pH was measured with a pH meter (868-2, Orion, Shanghai, China). Because the humic and tryptophan compounds in the target foulant have fluorescent excitation properties, the fluorescent compounds in the solution can be determined using the three-dimensional fluorescence excitation–emission matrix (EEM) spectra. A fluorescence spectrometer (F-7000, Hitachi, Tokyo, Japan) was used for determination. The excitation light (Ex) wavelength range was 200–450 nm, and the emission light (Em) wavelength range was 250–550 nm; the scanning intervals were 5 nm and 1 nm, respectively. The sample solution was filtered through a 0.45 μm microfiltration membrane, and the pH value was adjusted to 7.0 before the EEM test.

The contact angle of the liquid drops to the membrane surface was measured using a contact angle tester (JYSP-360, Beijing, China). Based on the extended Derjaguin–Landau–Verwey–Overbeek (XDLVO) theory, diiodomethane, ultrapure water, and glycerol were selected as test liquids to calculate the interfacial free energy. Computational methods of cohesion and adhesion free energy can be found in a previous work [35]. Scanning electron microscopy (Gemini SEM 300, Zeiss, Germany) was used to observe the morphology and microstructure of foulant particles on the ultrafiltration membrane surface, and the detailed working conditions were similar to those in previous studies [36,37].

3. Results

3.1. Effect of ClO_2 Pre-Oxidation on UF Membrane Fouling Alleviation

3.1.1. ClO_2 Pre-Oxidation for HA Fouling

The alleviating effect of ClO_2 pre-oxidation on ultrafiltration membrane fouling is shown in Figure 1. As shown in the figure, the decrease in membrane flux caused by raw humic acid water was more obvious than that after ClO_2 pre-oxidation. At the end of the first, second, and third filtration cycles, the specific flux (J/J_0) decreased to 0.36, 0.31, and 0.28, respectively. ClO_2 pre-oxidation significantly improved the flux, and the optimal flux mitigation was obtained when the dosage was 2 mg/L. At the end of each cycle of 2 mg/L ClO_2 , the specific flux J/J_0 rose to 0.45, 0.40, and 0.38, respectively. However, when the ClO_2 dosage was increased to 8 mg/L, the J/J_0 at the end of each filtration cycle was decreased to 0.41, 0.37, and 0.34, respectively. Compared with the dosage of 2 mg/L, the ability to recover J/J_0 at 8 mg/L was limited; thus, it could be seen that there was no positive correlation between ClO_2 dosage and flux recovery, which might be related to the membrane fouling mechanism [38].

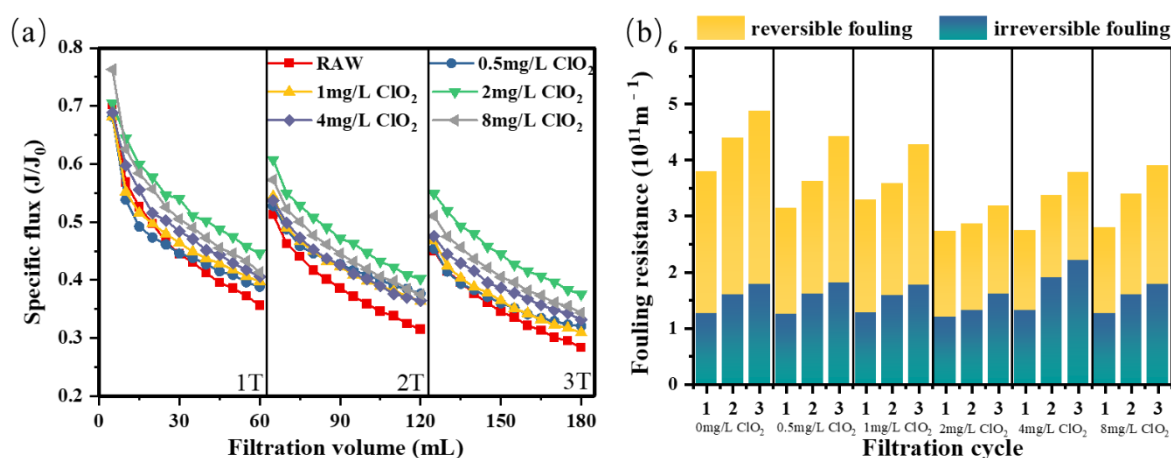


Figure 1. (a) Flux curve and (b) fouling resistance of the ultrafiltration membrane under different pre-oxidation dosages for HA.

In addition, after primary and secondary backwashing, the flow recovery rate was lower by 73% and 51%, respectively, indicating that the flow recovery rate of hydraulic backwashing was effectual, and that reversible fouling was dominant in HA fouling. As shown in Figure 1b, the total fouling resistance and reversible fouling resistance caused by raw humic acid water were the highest in the three cycles, and the total fouling resistance of different ClO_2 dosage groups decreased at first, and then increased over three filtration cycles, during which the optimal fouling resistance alleviation was achieved when the dosage was 2 mg/L. On the other hand, the proportion of irreversible fouling resistance increased, and the decline in the degree of resistance was relatively lower—even when the dosage was 4 mg/L, there was an increase at the end of the third filtration cycle. These results indicated that ClO_2 pre-oxidation had a good effect on improving permeate flux and alleviating reversible fouling during humic acid filtration, and that the filtration perfor-

mance might be reversely deteriorated when dosed with excessive ClO_2 . As experiments by Gan et al. showed, the yield of ClO_2 in humus depends on the dose and pH value of ClO_2 [39].

3.1.2. ClO_2 Pre-Oxidation for SA Fouling

As depicted in Figure 2a, the decrease in membrane flux caused by SA is more obvious than that caused by humic acid. The specific flux remained flat or even lower at the end of each cycle as the ClO_2 dose increased from 0 mg/L to 8 mg/L. When the ClO_2 dosage was 2 mg/L, although the flux decrease was relieved to some extent, the specific flux at the end of each filtration cycle was close to the value of sodium alginate raw water. Compared with humic acid, flux recovery of sodium alginate after hydraulic backwash was more apparent. As shown in Figure 2b, sodium alginate mainly caused severe reversible resistance, with a higher proportion than that in humic acid, which could be eliminated by high-intensity backwashing. With the dosage of ClO_2 above 2 mg/L, the irreversible fouling resistance decreased, indicating that ClO_2 pretreatment alleviated the irreversible fouling caused by sodium alginate to a certain extent. On the other hand, the reversible fouling caused by sodium alginate increased significantly with the dosing of ClO_2 , which was the most serious when the dosage was 8 mg/L, showing an increased reversible fouling resistance of $2.19 \times 10^{11} \text{ m}^{-1}$ compared with the sodium alginate raw water.

It could be seen that reversible fouling with pretreatment of ClO_2 played a leading role in membrane fouling induced by sodium alginate. This was consistent with previous research results, which could be attributed to the fact that sodium alginate can rapidly form a gel layer or cake layer on the membrane surface, causing membrane surface fouling [40].

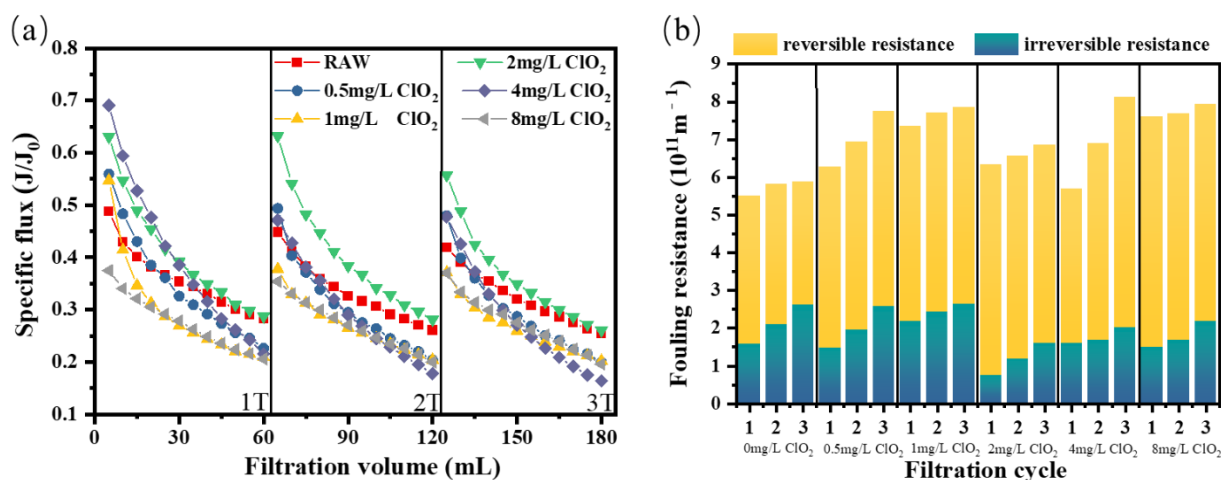


Figure 2. (a) Flux curve and (b) fouling resistance of the ultrafiltration membrane under different pre-oxidation dosages for SA.

3.1.3. ClO_2 Pre-Oxidation for BSA Fouling

The specific flux of different ClO_2 doses dropped sharply during the initial filtration cycle, after which the flux curve became smooth in the third cycle (Figure 3a). At the end of the first, second, and third filtration cycles, bovine serum protein caused a severe decrease in flux, with specific fluxes dropping to 0.46, 0.32, and 0.17, respectively. Moreover, the flux was difficult to recover after physical cleaning. Although the flux in each cycle increased slightly after hydraulic flushing with the dosing of ClO_2 , the flux decreased more significantly with the increase in the dose during the first two filtration cycles, indicating that ClO_2 pre-oxidation had no alleviating effect on flux reduction caused by bovine serum protein.

As shown in Figure 3b, irreversible and reversible fouling resistance caused by BSA at the end of filtration accounted for 62.8% and 27.2% of the total resistance, respectively. It could be concluded that irreversible resistance played the dominant role in membrane

fouling caused by bovine serum protein. Thus, the membrane flux was not well alleviated after hydraulic cleaning; however, after the pre-oxidation with ClO_2 (0.50–8 mg/L), both reversible and irreversible fouling were not only not alleviated, but even aggravated, at dosages below 1 mg/L. In addition, Cheng et al.’s experimental results also showed that lower doses of PMS as an oxidant aggravated membrane fouling by BSA [38]. These results indicate that ClO_2 pre-oxidation cannot improve the flux and reduce the fouling resistance during bovine serum albumin filtration. A possible reason for the limited fouling mitigation effect of pre-oxidation on BSA—especially compared to the mitigation effect for HA and SA—is the high molecular weight of BSA, which cannot be efficient degraded by a low-dosage oxidation process.

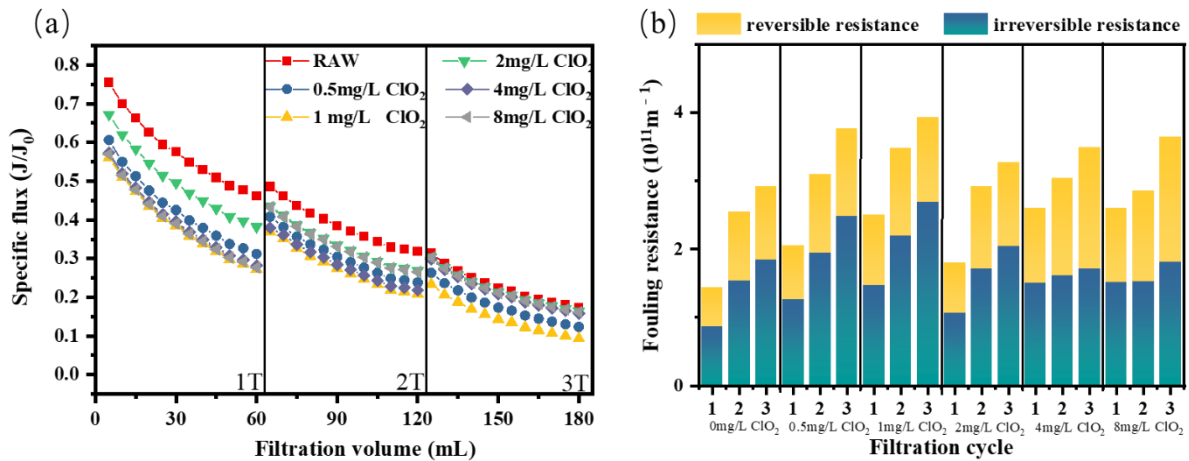


Figure 3. (a) Flux curve and (b) fouling resistance of the ultrafiltration membrane under different pre-oxidation dosages for BSA.

3.1.4. ClO_2 Pre-Oxidation for NOM Fouling

In actual water treatment, humus, proteins, and polysaccharides generally exist together. Therefore, in order to further explore the influence of ClO_2 as a pre-oxidant on membrane fouling caused by compound foulants, raw water mixed with humic acid, sodium alginate, and bovine serum protein was prepared. Figure 4 shows the influence of ClO_2 pre-oxidation on the membrane fouling of simulated natural water. At the end of three cycles of direct filtration, the specific flux of ultrafiltration membrane decreased to 0.11, 0.10, and 0.09, respectively. As can be seen from the figure, when the dose was 1 mg/L, ClO_2 pre-oxidation had the most obvious effect on improving flux compared with other doses, which was more prominent in the second and third filtration cycles.

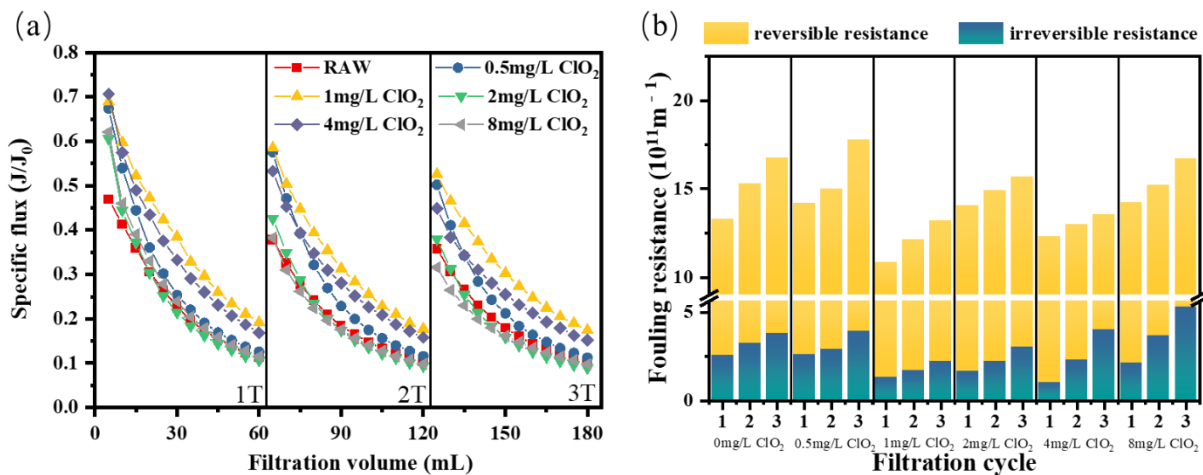


Figure 4. (a) Flux curve and (b) fouling resistance of the ultrafiltration membrane under different pre-oxidation dosages for NOM.

Unlike the treatment of model foulants, the membrane flux could be effectively recovered by hydraulic flushing. As shown in Figure 4b, similar to the treatment of raw water with individual forms of organic matter, the mitigation of membrane fouling was not improved with the increase in oxidizer dosage. On the contrary, low doses (1–4 mg/L) could effectively alleviate both reversible and irreversible resistance. These results showed that low ClO_2 pre-oxidation could not only improve the specific flux of mixed simulated natural water, but also reduce the membrane fouling—especially the irreversible fouling [41].

3.2. Effect of ClO_2 Pre-Oxidation on Purification Performance

Figure 5a shows the influence of pre-oxidation of ClO_2 at different dosages on DOC in raw water. As shown in the figure, with the increase in ClO_2 dosage (0.5–8 mg/L), the influent DOC values were 3.98 mg/L, 3.97 mg/L, 3.96 mg/L, 3.90 mg/L, and 3.51 mg/L, respectively. It was found that the dosing of ClO_2 caused a very limited improvement in DOC rejection, which is consistent with the results of previous studies on ozone degradation of organic foulants [41]. Compared with DOC removal, the UV_{254} value changed more obviously, which was because unsaturated bonds and aromatic rings preferentially reacted with oxidants and free radicals in water (Figure 5b) [42]. As shown in the figure, with the increase of ClO_2 dosage, the UV_{254} value of raw water decreased from 0.155 to 0.129, and the removal rate was 16.70%. When the dosage range of ClO_2 was between 2 and 8 mg/L, the absorbance remained virtually unchanged. In general, after adding ClO_2 , the removal rate of UV_{254} by the ultrafiltration membrane slightly decreased. When compared with previous work, it can be confirmed that ClO_2 oxidation has a better removal effect than chlorine oxidation in terms of DOC and UV_{254} [43].

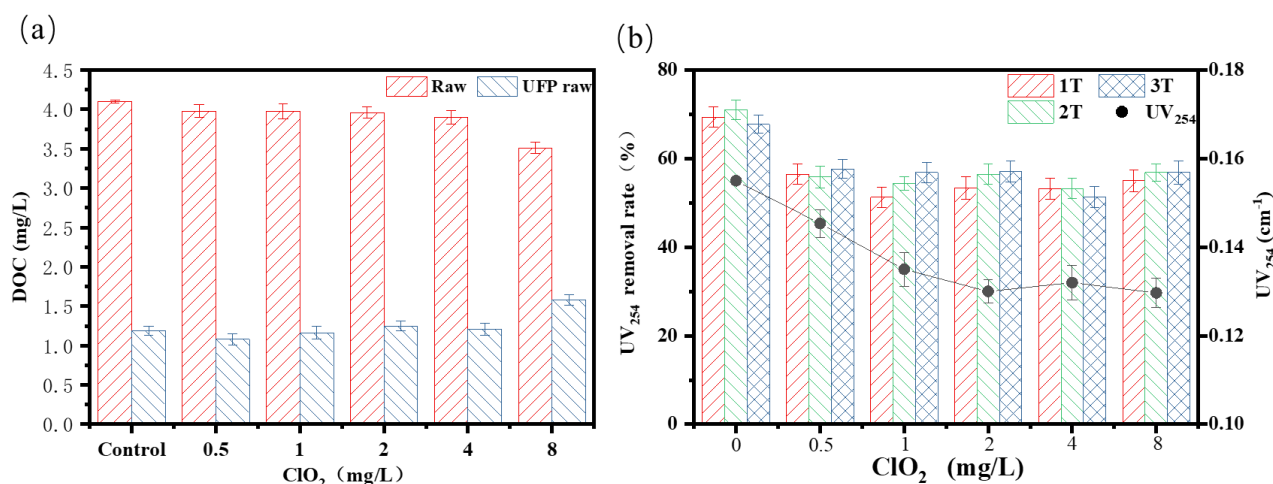


Figure 5. UV_{254} detection values and DOC concentrations at different dosages of pre-oxidation: (a) DOC; (b) UV_{254} .

The humic and tryptophan compounds in the target contaminant have fluorescent excitation properties. Therefore, these two substances in the solution can be determined using the EEM. Three-dimensional fluorescence spectra of effluents under different treatment conditions are shown in Figure 6. The three-dimensional fluorescence spectrograms have three distinct characteristic peaks: T, A, and C. The characteristic peaks of humus-like organics are generally considered as A and C, which mainly appear in the range of excitation wavelength 250–350 nm and emission wavelength 350–500 nm, while the characteristic peaks of tryptophan protein (T) mainly appear in the range of excitation wavelength 225–280 nm and emission wavelength 310–340 nm [44]. As shown in Figure 6a, humic acid raw water had an obvious characteristic peak A at $\text{Ex/Em} = 250\text{--}400/380\text{--}540$ nm, representing humus-like organics. When the dosage of ClO_2 was 2 mg/L, the fluorescence value of humus-like organics decreased. With the increase of ClO_2 dosage (4–8 mg/L), the

fluorescence response value of peak A increased appropriately, and reached a peak value at the dosage of 4 mg/L.

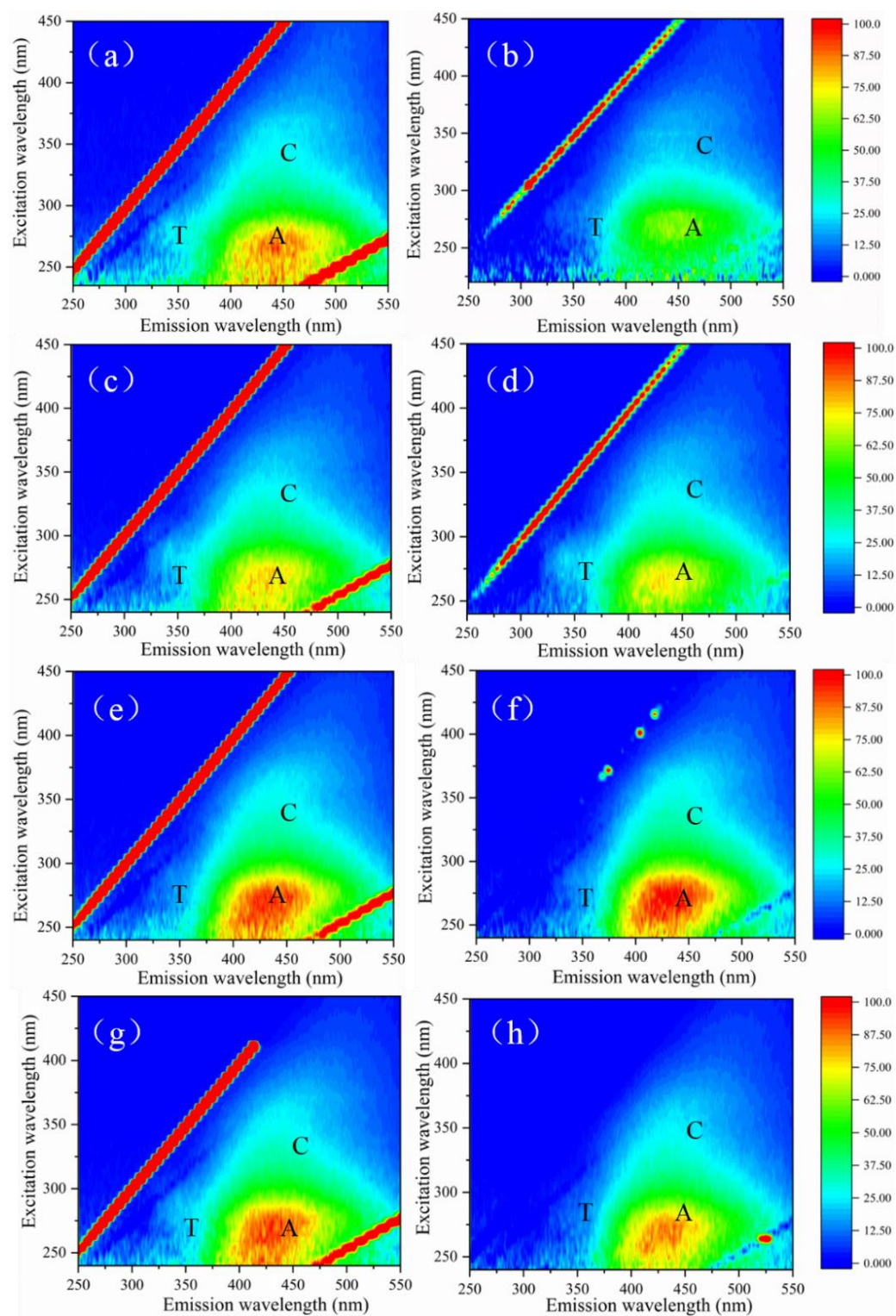


Figure 6. EEM spectra of samples under different pre-oxidation conditions: (a) humic acid raw water; (b) effluent of humic acid; (c) 2 mg/L ClO_2 pre-oxidation; (d) effluent of 2 mg/L ClO_2 pre-oxidation; (e) 4 mg/L ClO_2 pre-oxidation; (f) effluent of 4 mg/L ClO_2 pre-oxidation; (g) 8 mg/L ClO_2 pre-oxidation; (h) effluent of 8 mg/L ClO_2 pre-oxidation.

This study has shown that some functional groups that can stimulate fluorescence are hidden in humus water samples, and these hidden functional groups can be activated under the action of oxidants, resulting in the increase in the fluorescence values of humic analogs [45]. As can be seen from Figure 6b,d,f,h, peak A intensity weakened after filtration by the PES ultrafiltration membrane, indicating that the ultrafiltration membrane has certain interception and adsorption capacity for small-molecule humus-like organics that can stimulate fluorescence [46].

Figure 7 shows the effects of the ClO₂ ultrafiltration process on fluorescent substances of simulated natural water. As with the results of humic acid, the addition of ClO₂ reduced the intensity of peak A and produced an excitation effect on the fluorescent substances concealed in raw water. When the ClO₂ dose was 8 mg/L, peak A, representing humic substances, was significantly reduced, and the fluorescence value of peak A after UF was also lower than the other conditions, corresponding to the result of UV₂₅₄, indicating that the ClO₂ preferentially attacked unsaturated bonds and aromatic ring substances in humic acids [42].

3.3. Effect of ClO₂ Pre-Oxidation on Interface Characteristics and Fouling Mechanisms

The surface of the ultrafiltration membrane was characterized by scanning electron microscope (SEM), and the mechanism of ultrafiltration membrane fouling caused by ClO₂ was further analyzed by fitting the interfacial free energy and membrane fouling model. As shown in Figure 8a, the surface of the original ultrafiltration membrane was clean and smooth, with no accumulation of foulant. However, after filtration of humic acid and simulated natural water, the surface morphology of the membrane was obviously different due to the accumulation of foulants [38]. The membrane surfaces after filtration of HA and simulated natural water are shown in Figure 8b,e, respectively, where we can observe obvious particle deposition on the membrane surfaces and a relatively dense fouling layer/cake layer. Figure 8c,d show the SEM images of membrane surfaces having filtered pre-oxidized humic acid solution with ClO₂ dosages of 2 mg/L and 8 mg/L, respectively. It can be seen that compared with Figure 8b, the membrane surface of the two pretreatment conditions was relatively smooth, and the surface foulant particles were also reduced in quantity.

As shown in Figure 8f, when the dosage of ClO₂ was 2 mg/L, the foulants on the membrane surface had a boundary outline except for a few places, and the rest of the membrane surface was relatively smooth. When the ClO₂ dosage was 8 mg/L, the membrane surface showed a large accumulation of foulants; this may have been due to the agglomeration of organic substances in raw water after pre-oxidation, which reduced the membrane water capacity and increased the membrane resistance, which was not conducive to the stable operation of the membrane.

The XDLVO theory was used for interface analysis, and the condensation free energy and adhesion free energy of the ultrafiltration membrane surface with various ClO₂ doses were calculated. The results are shown in Tables 1 and 2, in which ΔG^{LW} , ΔG^{AB} , and ΔG^{EL} are the van der Waals force condensation/adhesion free energy, polar force condensation/adhesion free energy, and electrostatic condensation/adhesion free energy, respectively. In addition, ΔG_{131} represents the condensation free energy between the interfaces, ΔG_{132} represents the adhesion free energy of the interface, and their values are calculated through the various interface forces. " $\Delta G > 0$ " indicates that the material interface is in a stable state, which is repulsive; " $\Delta G < 0$ " indicates that the material interface is in an unstable state, and is attractive [47]. As shown in Table 1, ΔG^{LW} and ΔG^{EL} slightly changed with the increase in ClO₂ dosage, indicating that polar force dominated. In addition, the ΔG_{131} was -5.36 mJ/m^2 , ΔG^{AB} was -1.63 mJ/m^2 , and the value of ΔG^{AB} increased to 14.10 mJ/m^2 with the increase in the ClO₂ dose (from 2 mg/L to 8 mg/L), indicating that the surface polarity increased and the hydrophilicity was improved. However, when ClO₂ was added, the adhesion free energy of ΔG_{132} between humic acid and the UF

membrane increased from -8.28 to 8.91 , indicating that the attraction between humic acid and the UF membrane changed to repulsion.

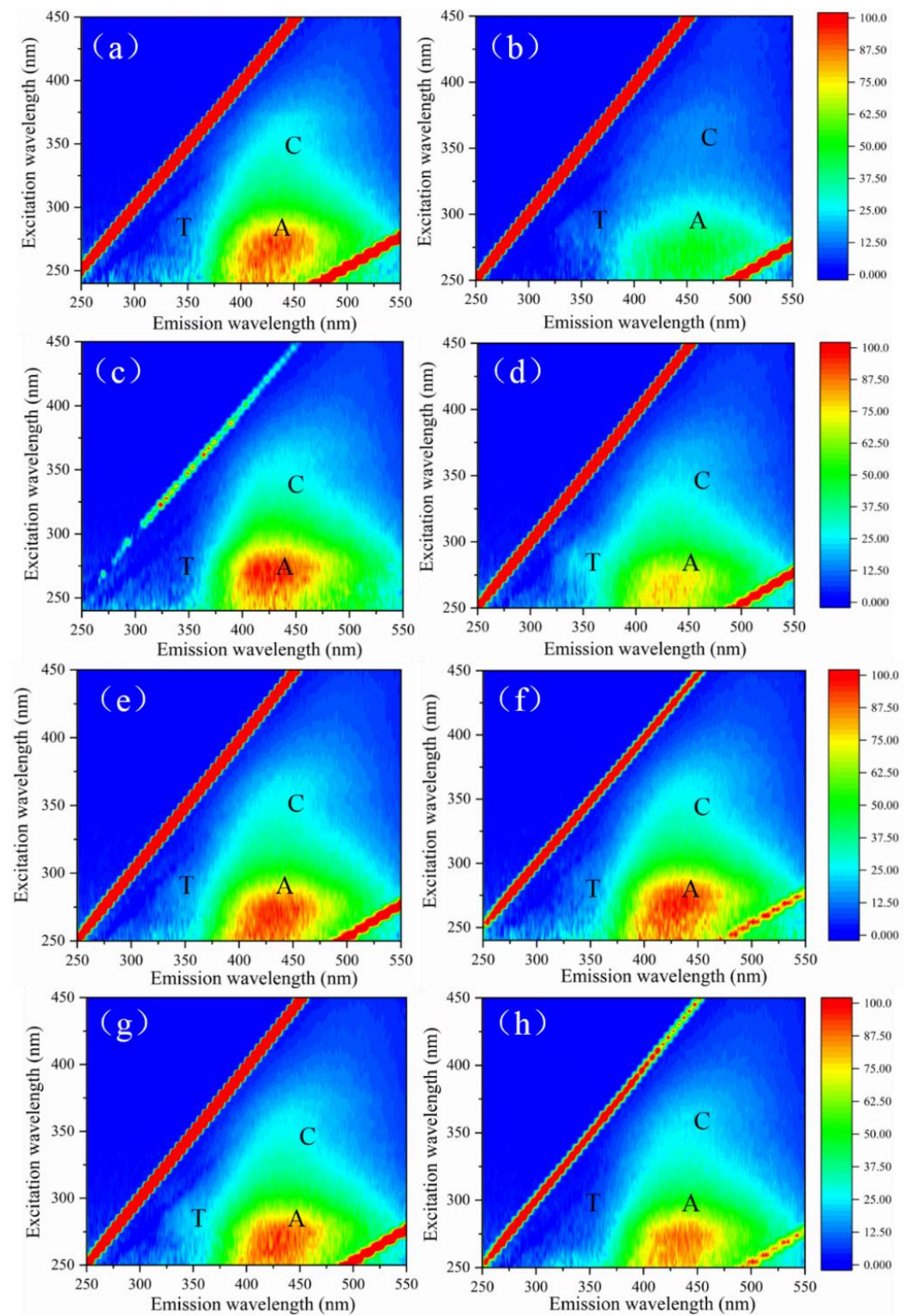


Figure 7. EEM spectra of samples under different pre-oxidation conditions: (a) simulated natural water; (b) effluent of simulated natural water; (c) 1 mg/L ClO_2 pre-oxidation; (d) effluent of 1 mg/L ClO_2 pre-oxidation; (e) 4 mg/L ClO_2 pre-oxidation; (f) effluent of 4 mg/L ClO_2 pre-oxidation; (g) 8 mg/L ClO_2 pre-oxidation; (h) effluent of 8 mg/L ClO_2 pre-oxidation.

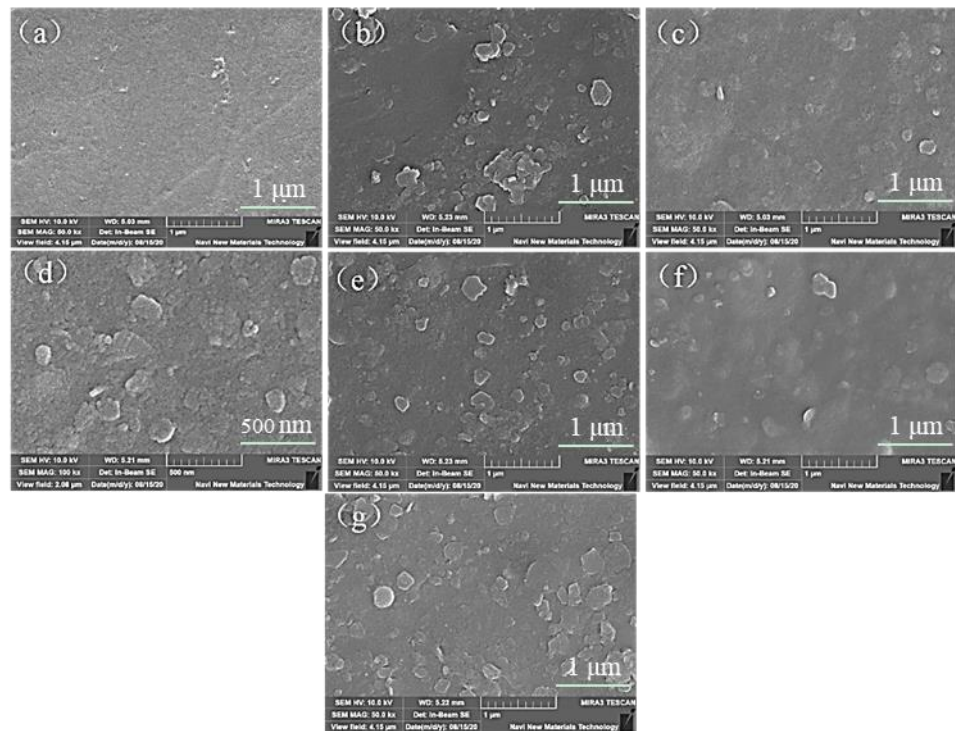


Figure 8. SEM images of pollutant morphology on membrane surfaces under different ClO₂ dosages: (a) pristine membrane; (b) membrane having filtered humic acid; (c) membrane having filtered humic acid after 2 mg/L ClO₂ pre-oxidation; (d) membrane having filtered humic acid after 8 mg/L ClO₂ pre-oxidation; (e) membrane having filtered simulated natural water; (f) membrane having filtered simulated natural water after 2 mg/L ClO₂ pre-oxidation; (g) membrane having filtered simulated natural water after 8 mg/L ClO₂ pre-oxidation.

Table 1. Free energy of interfacial condensation and adhesion of the ultrafiltration membrane surface, caused by humic acid (mJ/m²).

Dosage (mg/L)	ΔG_{131}^{LW}	ΔG_{131}^{AB}	ΔG_{131}^{EL}	ΔG_{131}	ΔG_{132}^{LW}	ΔG_{132}^{AB}	ΔG_{132}^{EL}	ΔG_{132}
0	−3.75	−1.63	0.12	−5.36	−4.23	−4.02	−0.03	−8.28
2	−4.25	9.22	0.08	5.05	−4.50	14.07	−0.01	9.96
4	−4.76	13.24	0.05	8.53	−4.76	11.07	0.02	8.23
8	−5.28	14.10	0.02	8.90	−5.01	13.89	0.03	8.91

Table 2. Interfacial condensation free energy and adhesion free energy of the ultrafiltration membrane surface, caused by simulated natural water (mJ/m²).

Dosage (mg/L)	ΔG_{131}^{LW}	ΔG_{131}^{AB}	ΔG_{131}^{EL}	ΔG_{131}	ΔG_{132}^{LW}	ΔG_{132}^{AB}	ΔG_{132}^{EL}	ΔG_{132}
0	−2.37	−6.03	0.11	−8.29	−3.36	1.30	−0.02	−2.04
1	−5.28	10.63	0.06	5.41	−5.01	14.85	0.02	9.89
4	−5.54	8.43	0.02	2.91	−5.14	13.19	0.03	8.11
8	−5.80	−7.35	−0.01	−13.16	−5.46	5.29	0.10	−0.07

As shown in Table 2, the ΔG^{EL} and ΔG^{LW} between the ultrafiltration membrane and the simulated natural water did not change much with the dosage of ClO₂, which was still dominated by polar force. When the ClO₂ dosage was 8 mg/L, unlike with humic acid, the value of ΔG_{131} was −13.16 mJ/m², indicating that the foulants were in a state of mutual attraction. At the same time, the value of ΔG_{132} was −0.07 mJ/m², indicating that the adhesion free energy between the foulants and the membrane was small and attractive, facilitating deposition on the membrane surface. This confirmed that the obvious

foulant profile of the simulated natural water on the membrane surface in the SEM figure was the result of mutual attraction between the mechanical mixture and the ultrafiltration membrane, and was consistent with the obvious attenuation of membrane flux and serious membrane fouling.

In order to further investigate the effect of ClO₂ pretreatment on the membrane fouling mechanism, the membrane fouling model based on d^2t/dV^2 and dt/dV (Ho and ZyD-Ney, 2000) was adopted, where the t and V represent the membrane filtration time and the total membrane filtration volume, respectively. As can be seen from Figure 9, the values of “ D^2 ”, “ T/D ”, “ V^2 ”, and “ DT/dV ” decreased significantly after ClO₂ pre-oxidation. However, the value of “ DT/dV ” increased during the treatment of BSA, indicating that the filtration time increased during ultrafiltration. It was confirmed that severe membrane fouling was produced during the pretreatment of BSA with ClO₂, which is consistent with its flux curve.

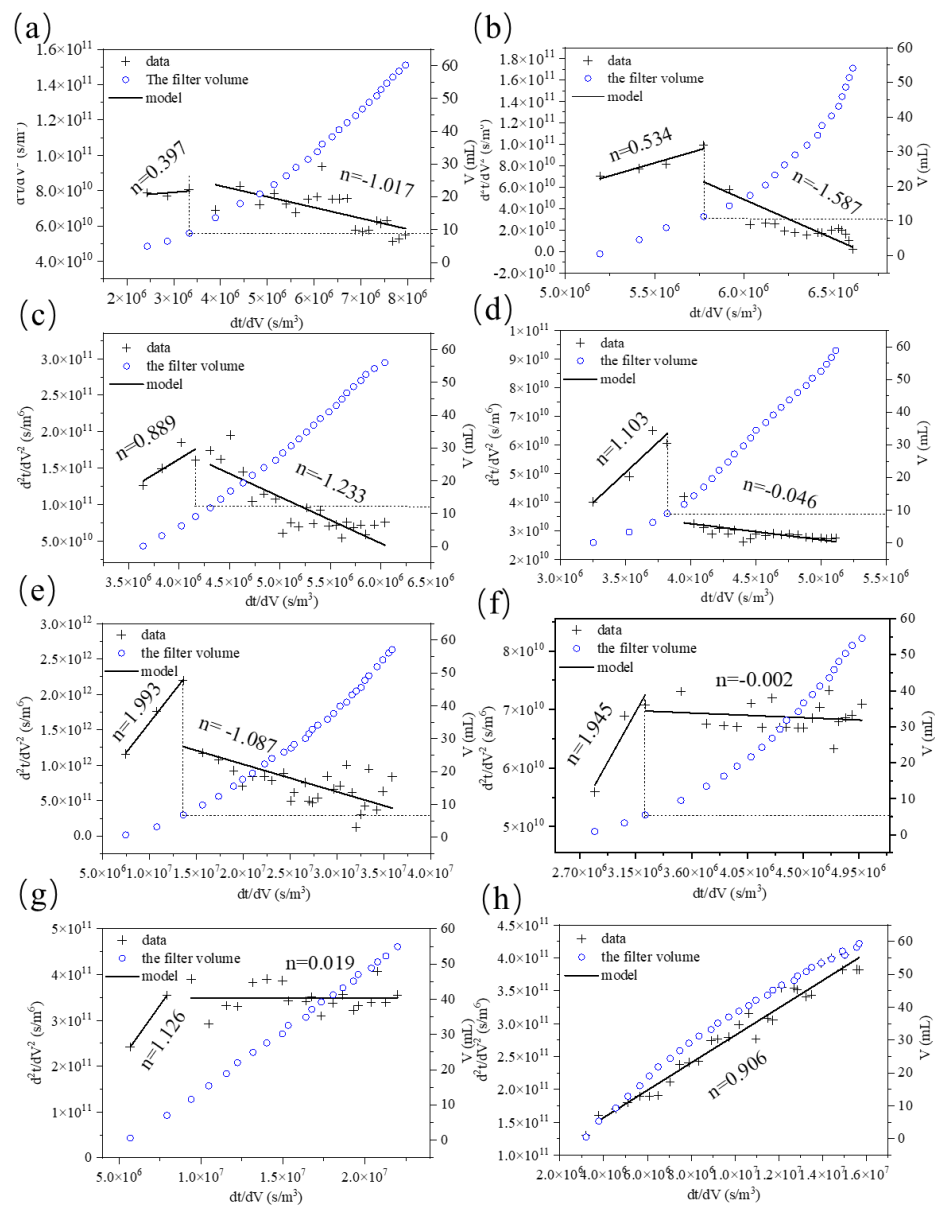


Figure 9. Data and fitting curves (membrane d^2t/dV^2 and dt/dV) for ultrafiltration of organic foulants with different ClO₂ dosages: (a) HA without pre-oxidation; (b) HA with 2 mg/L ClO₂ pre-oxidation; (c) SA without pre-oxidation; (d) SA with 2 mg/L ClO₂ pre-oxidation; (e) BSA without pre-oxidation; (f) BSA with 2 mg/L ClO₂ pre-oxidation; (g) simulated natural water without pre-oxidation; (h) simulated natural water with 2 mg/L ClO₂ pre-oxidation.

As shown in Figure 9a, the n value of HA without pre-oxidation was 0.40 at the initial stage of filtration, and -1.02 at the later stage of filtration. At this time, the fouling mechanism of the membrane surface caused by the blocking of membrane holes changed [48], which is consistent with Wang's results of UV/chlorine treatment of humic acid [43]. It could be concluded that the membrane fouling mechanism was mainly a result of membrane hole blockage and the cake layer. Figure 9b shows the fitting curve of HA after pre-oxidation with 2 mg/L ClO_2 ; it can be seen that the fitting curve is similar to that in Figure 9a, indicating that the fouling mechanism was consistent with and without ClO_2 pre-oxidation. When SA was pre-oxidized at 2 mg/L ClO_2 , the membrane fouling mechanism was not changed, although the fouling was alleviated. It is noteworthy that after oxidizing simulated natural water with 2 mg/L ClO_2 , the fouling mechanism changed from cake layer fouling to critical blocking, which alleviated membrane fouling.

4. Conclusions

In this work, the effects of ClO_2 pre-oxidation on the treatment of various typical organic foulants—and their mixture simulating natural water—with an ultrafiltration membrane were investigated, and the fouling mechanism was analyzed by membrane surface morphology, interfacial free energy, and membrane fouling models. It was found that this method was not only low-cost and easy to operate, but also could effectively alleviate membrane fouling caused by simulated natural water in the appropriate dosage range. The main conclusions are as follows:

ClO_2 pre-oxidation at a lower concentration (1–2 mg/L) can alleviate the decrease in membrane flux caused by humus, polysaccharides, and mixed organic foulants, among which the highest traffic recovery rate reached 73%, 89%, and 86%, respectively, although its effect in terms of reducing membrane irreversible resistance was limited. In addition, the experimental results showed that ClO_2 pre-oxidation faced some difficulty in alleviating the membrane flux decrease caused by protein substances. Furthermore, the removal effect of DOC in raw humic acid water by ClO_2 dosing was not ideal. ClO_2 oxidation activated the hidden functional groups in the raw water, resulting in an increase in the fluorescence value of humic analogs and a good removal effect on the fluorescence intensity of BSA. In general, the dosage of ClO_2 was inversely proportional to the mitigation effect of membrane fouling, as well as the irreversible fouling, in the treatment of simulated natural water.

The interfacial free energy analysis showed that the attraction between organics increased, and they easily deposited onto the membrane surface, resulting in a serious flux decline and membrane resistance increase when the dosage was 8 mg/L. However, at 1 mg/L pre-oxidation, the polarity force between the membrane and organic matter could be improved, thus increasing the repulsion force and, in turn, alleviating membrane fouling.

The fitting results of the membrane fouling model showed that ClO_2 could not effectively change the fouling mechanism caused by typical organic matter in water, and that the pre-oxidation of BSA could accelerate the formation of the cake layer, thus prolonging the membrane filtration duration. However, at a low concentration (1 mg/L), the membrane fouling mechanism induced by simulated natural water could change from standard blocking and cake layer blocking to critical blocking.

Author Contributions: Conceptualization, Z.S.; methodology, K.Y.; software, K.Y.; validation, B.L. and M.W.; formal analysis, K.Y.; investigation, B.L.; data curation, M.W.; writing—original draft preparation, B.L.; writing—review and editing, K.Y. and G.L.; funding acquisition, B.L. All authors have read and agreed to the published version of the manuscript.

Funding: This work was financially supported by the National Natural Science Foundation of China (52000062).

Institutional Review Board Statement: Not applicable.

Informed Consent Statement: Not applicable.

Data Availability Statement: Some or all data, models, or code that support the findings of this study are available from the corresponding author upon reasonable request.

Conflicts of Interest: The authors declare no conflict of interest.

References

1. Santschi, P.; Xu, C.; Zhang, S.; Schwehr, K.A.; Lin, P.; Yeager, C.; Kaplan, D. Recent advances in the detection of specific natural organic compounds as carriers for radionuclides in soil and water environments, with examples of radioiodine and plutonium. *J. Environ. Radioact.* **2017**, *171*, 226–233. [CrossRef]
2. Lipczynska-Kochany, E. Effect of climate change on humic substances and associated impacts on the quality of surface water and groundwater: A review. *Sci. Total Environ.* **2018**, *640–641*, 1548–1565. [CrossRef]
3. Williamson, C.E.; Madronich, S.; Lal, A.; Zepp, R.G.; Lucas, R.M.; Overholt, E.P.; Rose, K.C.; Schladow, S.G.; Lee-Taylor, J. Climate change-induced increases in precipitation are reducing the potential for solar ultraviolet radiation to inactivate pathogens in surface waters. *Sci. Rep.* **2017**, *7*, 13033. [CrossRef]
4. Bond, T.; Goslan, E.; Parsons, S.; Jefferson, B. Treatment of disinfection by-product precursors. *Environ. Technol.* **2011**, *32*, 1–25. [CrossRef]
5. Pettit, R.E. Organic Matter, Humus, Humate, Humic Acid, Fulvic Acid. 2008. Available online: <http://www.harvestgrow.com/pdf%20web%20site/Humates%20General%20Info.pdf> (accessed on 1 June 2021).
6. Matilainen, A.; Gjessing, E.T.; Lahtinen, T.; Hed, L.; Bhatnagar, A.; Sillanpää, M. An overview of the methods used in the characterisation of natural organic matter (NOM) in relation to drinking water treatment. *Chemosphere* **2011**, *83*, 1431–1442. [CrossRef]
7. Tang, W.-W.; Zeng, G.-M.; Gong, J.-L.; Liang, J.; Xu, P.; Zhang, C.; Huang, B. Impact of humic/fulvic acid on the removal of heavy metals from aqueous solutions using nanomaterials: A review. *Sci. Total Environ.* **2014**, *468–469*, 1014–1027. [CrossRef]
8. Matilainen, A.; Vepsäläinen, M.; Sillanpää, M. Natural organic matter removal by coagulation during drinking water treatment: A review. *Adv. Colloid Interface Sci.* **2010**, *159*, 189–197. [CrossRef]
9. Zhu, T.; Qu, F.; Liu, B.; Liang, H. The influence of environmental factor on the coagulation enhanced ultrafiltration of algae-laden water: Role of two anionic surfactants to the separation performance. *Chemosphere* **2021**, 132745. [CrossRef]
10. Genz, A.; Baumgarten, B.; Goernitz, M.; Jekel, M. NOM removal by adsorption onto granular ferric hydroxide: Equilibrium, kinetics, filter and regeneration studies. *Water Res.* **2008**, *42*, 238–248. [CrossRef]
11. Matilainen, A.; Sillanpää, M. Removal of natural organic matter from drinking water by advanced oxidation processes. *Chemosphere* **2010**, *80*, 351–365. [CrossRef]
12. Metsämuuronen, S.; Sillanpää, M.; Bhatnagar, A.; Mänttari, M. Natural Organic Matter Removal from Drinking Water by Membrane Technology. *Sep. Purif. Rev.* **2014**, *43*, 1–61. [CrossRef]
13. Zhu, T.; Zhou, Z.; Qu, F.; Liu, B.; Van der Bruggen, B. Separation performance of ultrafiltration during the separation of algae-laden water in the presence of an anionic surfactant. *Sep. Purif. Technol.* **2021**, *281*, 119894. [CrossRef]
14. Li, G.; Liu, B.; Bai, L.; Shi, Z.; Tang, X.; Wang, J.; Liang, H.; Zhang, Y.; Van der Bruggen, B. Improving the performance of loose nanofiltration membranes by poly-dopamine/zwitterionic polymer coating with hydroxyl radical activation. *Sep. Purif. Technol.* **2019**, *238*, 116412. [CrossRef]
15. Qu, F.; Cao, A.; Yang, Y.; Mahmud, S.; Su, P.; Yang, J.; He, Z.; Lai, Q.; Zhu, L.; Tu, Z.; et al. Hierarchically superhydrophilic poly(vinylidene fluoride) membrane with self-cleaning fabricated by surface mineralization for stable separation of oily wastewater. *J. Membr. Sci.* **2021**, *640*, 119864. [CrossRef]
16. Khan, N.; Niazi, M.; Sher, F.; Jahan, Z.; Noor, T.; Azhar, O.; Rashid, T.; Iqbal, N. Metal Organic Frameworks Derived Sustainable Polyvinyl Alcohol/Starch Nanocomposite Films as Robust Materials for Packaging Applications. *Polymers* **2021**, *13*, 2307. [CrossRef] [PubMed]
17. Ali, M.; Jahan, Z.; Sher, F.; Niazi, M.B.K.; Kakar, S.J.; Gul, S. Nano architected cues as sustainable membranes for ultrafiltration in blood hemodialysis. *Mater. Sci. Eng. C* **2021**, *128*, 112260. [CrossRef]
18. Azhar, O.; Jahan, Z.; Sher, F.; Niazi, M.B.K.; Kakar, S.J.; Shahid, M. Cellulose acetate-polyvinyl alcohol blend hemodialysis membranes integrated with dialysis performance and high biocompatibility. *Mater. Sci. Eng. C* **2021**, *126*, 112127. [CrossRef]
19. Obotey Ezugbe, E.; Rathilal, S. Membrane Technologies in Wastewater Treatment: A Review. *Membranes* **2020**, *10*, 89. [CrossRef]
20. Shao, S.; Fu, W.; Li, X.; Shi, D.; Jiang, Y.; Li, J.; Gong, T.; Li, X. Membrane fouling by the aggregations formed from oppositely charged organic foulants. *Water Res.* **2019**, *159*, 95–101. [CrossRef]
21. Liu, B.; Qu, F.; Yu, H.; Tian, J.; Chen, W.; Liang, H.; Li, G.; Van der Bruggen, B. Membrane Fouling and Rejection of Organics during Algae-Laden Water Treatment Using Ultrafiltration: A Comparison between in Situ Pretreatment with Fe(II)/Persulfate and Ozone. *Environ. Sci. Technol.* **2018**, *52*, 765–774. [CrossRef]
22. Yan, P.; Chen, Z.; Wang, S.; Zhou, Y.; Li, L.; Yuan, L.; Shen, J.; Jin, Q.; Zhang, X.; Kang, J. Catalytic ozonation of iohexol with α -Fe_{0.9}Mn_{0.1}OOH in water: Efficiency, degradation mechanism and toxicity evaluation. *J. Hazard. Mater.* **2020**, *402*, 123574. [CrossRef] [PubMed]

23. He, Q.; Xie, Z.; Tang, M.; Fu, Z.; Ma, J.; Wang, H.; Zhang, W.; Zhang, H.; Wang, M.; Hu, J.; et al. Insights into the simultaneous nitrification, denitrification and phosphorus removal process for in situ sludge reduction and potential phosphorus recovery. *Sci. Total Environ.* **2021**, *801*, 149569. [[CrossRef](#)] [[PubMed](#)]
24. He, Q.; Xie, Z.; Fu, Z.; Wang, M.; Xu, P.; Yu, J.; Ma, J.; Gao, S.; Chen, L.; Zhang, W.; et al. Interaction and removal of oxytetracycline with aerobic granular sludge. *Bioresour. Technol.* **2020**, *320*, 124358. [[CrossRef](#)] [[PubMed](#)]
25. Gan, W.; Ge, Y.; Zhu, H.; Huang, H.; Yang, X. ClO₂ pre-oxidation changes the yields and formation pathways of chloroform and chloral hydrate from phenolic precursors during chlorination. *Water Res.* **2018**, *148*, 250–260. [[CrossRef](#)]
26. He, G.; Zhang, T.; Zhang, Q.; Dong, F.; Wang, Y. Characterization of enoxacin (ENO) during ClO₂ disinfection in water distribution system: Kinetics, byproducts, toxicity evaluation and halogenated disinfection byproducts (DBPs) formation potential. *Chemosphere* **2021**, *283*, 131251. [[CrossRef](#)] [[PubMed](#)]
27. Zhong, Y.; Gan, W.; Du, Y.; Huang, H.; Wu, Q.; Xiang, Y.; Shang, C.; Yang, X. Disinfection byproducts and their toxicity in wastewater effluents treated by the mixing oxidant of ClO₂/Cl₂. *Water Res.* **2019**, *162*, 471–481. [[CrossRef](#)]
28. Shao, K.-L.; Ye, Z.-X.; Huang, H.; Yang, X. ClO₂ pre-oxidation impacts the formation and nitrogen origins of dichloroacetonitrile and dichloroacetamide during subsequent chloramination. *Water Res.* **2020**, *186*, 116313. [[CrossRef](#)]
29. Gan, W.; Ge, Y.; Zhong, Y.; Yang, X. The reactions of chlorine dioxide with inorganic and organic compounds in water treatment: Kinetics and mechanisms. *Environ. Sci. Technol.* **2020**, *6*, 2287–2312. [[CrossRef](#)]
30. Zhang, Y.; Fu, Q. Algal fouling of microfiltration and ultrafiltration membranes and control strategies: A review. *Sep. Purif. Technol.* **2018**, *203*, 193–208. [[CrossRef](#)]
31. Tian, J.-Y.; Ernst, M.; Cui, F.; Jekel, M. Effect of particle size and concentration on the synergistic UF membrane fouling by particles and NOM fractions. *J. Membr. Sci.* **2013**, *446*, 1–9. [[CrossRef](#)]
32. Her, N.; Amy, G.; Foss, D.; Cho, J. Variations of Molecular Weight Estimation by HP-Size Exclusion Chromatography with UVA versus Online DOC Detection. *Environ. Sci. Technol.* **2002**, *36*, 3393–3399. [[CrossRef](#)] [[PubMed](#)]
33. Ho, C.C.; Zydney, A.L. A Combined Pore Blockage and Cake Filtration Model for Protein Fouling during Microfiltration. *J. Colloid Interface Sci.* **2000**, *232*, 389–399. [[CrossRef](#)]
34. Huang, H.; Young, T.A.; Jacangelo, J.G. Unified Membrane Fouling Index for Low Pressure Membrane Filtration of Natural Waters: Principles and Methodology. *Environ. Sci. Technol.* **2007**, *42*, 714–720. [[CrossRef](#)]
35. Liu, B.; Qu, F.; Liang, H.; Gan, Z.; Yu, H.; Li, G.; Van der Bruggen, B. Algae-laden water treatment using ultrafiltration: Individual and combined fouling effects of cells, debris, extracellular and intracellular organic matter. *J. Membr. Sci.* **2017**, *528*, 178–186.
36. Altaf, F.; Niazi, M.B.K.; Jahan, Z.; Ahmad, T.; Akram, M.A.; Safdar, A.; Butt, M.S.; Noor, T.; Sher, F. Synthesis and Characterization of PVA/Starch Hydrogel Membranes Incorporating Essential Oils Aimed to be Used in Wound Dressing Applications. *J. Polym. Environ.* **2020**, *29*, 156–174. [[CrossRef](#)]
37. Jubeen, F.; Liaqat, A.; Sultan, M.; Iqbal, S.Z.; Sajid, I.; Sher, F. Green synthesis and biological evaluation of novel 5-fluorouracil derivatives as potent anticancer agents. *Saudi Pharm. J.* **2019**, *27*, 1164–1173. [[CrossRef](#)]
38. Cheng, X.; Liang, H.; Ding, A.; Tang, X.; Liu, B.; Zhu, X.; Gan, Z.; Wu, D.; Li, G. Ferrous iron/peroxymonosulfate oxidation as a pretreatment for ceramic ultrafiltration membrane: Control of natural organic matter fouling and degradation of atrazine. *Water Res.* **2017**, *113*, 32–41. [[CrossRef](#)]
39. Gan, W.; Huang, S.; Ge, Y.; Bond, T.; Westerhoff, P.; Zhai, J.; Yang, X. Chlorite formation during ClO₂ oxidation of model compounds having various functional groups and humic substances. *Water Res.* **2019**, *159*, 348–357. [[CrossRef](#)]
40. Li, K.; Liang, H.; Qu, F.; Shao, S.; Yu, H.; Han, Z.-S.; Du, X.; Li, G. Control of natural organic matter fouling of ultrafiltration membrane by adsorption pretreatment: Comparison of mesoporous adsorbent resin and powdered activated carbon. *J. Membr. Sci.* **2014**, *471*, 94–102. [[CrossRef](#)]
41. Cheng, X.; Liang, H.; Ding, A.; Qu, F.; Shao, S.; Liu, B.; Wang, H.; Wu, D.; Li, G. Effects of pre-ozonation on the ultrafiltration of different natural organic matter (NOM) fractions: Membrane fouling mitigation, prediction and mechanism. *J. Membr. Sci.* **2016**, *505*, 15–25. [[CrossRef](#)]
42. Chong, M.N.; Jin, B.; Chow, C.W.K.; Saint, C. Recent developments in photocatalytic water treatment technology: A review. *Water Res.* **2010**, *44*, 2997–3027. [[CrossRef](#)]
43. Wan, Y.; Xie, P.; Wang, Z.; Wang, J.; Ding, J.; Dewil, R.; Van der Bruggen, B. Application of UV/chlorine pretreatment for controlling ultrafiltration (UF) membrane fouling caused by different natural organic fractions. *Chemosphere* **2020**, *263*, 127993. [[CrossRef](#)]
44. Liu, B.; Qu, F.; Chen, W.; Liang, H.; Wang, T.; Cheng, X.; Yu, H.; Li, G.; Van der Bruggen, B. Microcystis aeruginosa-laden water treatment using enhanced coagulation by persulfate/Fe(II), ozone and permanganate: Comparison of the simultaneous and successive oxidant dosing strategy. *Water Res.* **2017**, *125*, 72–80. [[CrossRef](#)] [[PubMed](#)]
45. Chen, W.; Westerhoff, P.; Leenheer, J.A.; Booksh, K. Fluorescence Excitation–Emission Matrix Regional Integration to Quantify Spectra for Dissolved Organic Matter. *Environ. Sci. Technol.* **2003**, *37*, 5701–5710. [[CrossRef](#)]
46. Xing, J.; Wang, H.; Cheng, X.; Tang, X.; Luo, X.; Wang, J.; Wang, T.; Li, G.; Liang, H. Application of low-dosage UV/chlorine pre-oxidation for mitigating ultrafiltration (UF) membrane fouling in natural surface water treatment. *Chem. Eng. J.* **2018**, *344*, 62–70. [[CrossRef](#)]

-
47. Lee, S.; Kim, S.; Cho, J.; Hoek, E.M.V. Natural organic matter fouling due to foulant–membrane physicochemical interactions. *Desalination* **2007**, *202*, 377–384. [[CrossRef](#)]
 48. Byun, S.; Taurozzi, J.S.; Alpatova, A.L.; Wang, F.; Tarabara, V.V. Performance of polymeric membranes treating ozonated surface water: Effect of ozone dosage. *Sep. Purif. Technol.* **2011**, *81*, 270–278. [[CrossRef](#)]